www.sciencemag.org/content/360/6389/621/suppl/DC1

Supplementary Materials for

Recent Asian origin of chytrid fungi causing global amphibian declines

Simon J. O'Hanlon,* Adrien Rieux, Rhys A. Farrer, Gonçalo M. Rosa, Bruce Waldman, Arnaud Bataille, Tiffany A. Kosch, Kris A. Murray, Balázs Brankovics, Matteo Fumagalli, Michael D. Martin, Nathan Wales, Mario Alvarado-Rybak, Kieran A. Bates, Lee Berger, Susanne Böll, Lola Brookes, Frances Clare, Elodie A. Courtois, Andrew A. Cunningham, Thomas M. Doherty-Bone, Pria Ghosh, David J. Gower, William E. Hintz, Jacob Höglund, Thomas S. Jenkinson, Chun-Fu Lin, Anssi Laurila, Adeline Loyau, An Martel, Sara Meurling, Claude Miaud, Pete Minting, Frank Pasmans, Dirk S. Schmeller, Benedikt R. Schmidt, Jennifer M. G. Shelton, Lee F. Skerratt, Freya Smith, Claudio Soto-Azat, Matteo Spagnoletti, Giulia Tessa, Luís Felipe Toledo, Andrés Valenzuela-Sánchez, Ruhan Verster, Judit Vörös, Rebecca J. Webb, Claudia Wierzbicki, Emma Wombwell, Kelly R. Zamudio, David M. Aanensen, Timothy Y. James, M. Thomas P. Gilbert, Ché Weldon, Jaime Bosch, François Balloux, Trenton W. J. Garner, Matthew C. Fisher*

*Corresponding author. Email: simon.ohanlon@gmail.com (S.J.O.); matthew.fisher@imperial.ac.uk (M.C.F.)

Published 11 May 2018, *Science* **360**, 621 (2018)
DOI: 10.1126/science.aar1965

This PDF file includes:

Other supplementary material for this manuscript includes:

Figures S2, S5, and S8

Table S1 (Excel format)

Data S1 to S3 (zipped archive)

Materials and Methods

DNA extraction and sequencing library preparation

Isolate collection and subsequent sequencing was performed over several years, using multiple DNA extraction methods, different versions of library preparation kit chemistries and at different sequencing centres. Newly sequenced isolates for this study were grown in 50ml Nalgene Nunc™ tissue culture-treated flasks (Thermo Fisher Scientific, Massachusetts, USA) for 10-14 days at 18-20℃. DNA extraction was performed using the MasterPure™ Yeast DNA Purification Kit (Epicentre, Wisconsin, USA) or Qiagen Genomic Tips 20/G and DNeasy™ Blood and Tissue Kits (Qiagen, Venlo, Netherlands). DNA extractions were quantified using a Tapestation™ 2200 (Agilent Technologies, California, United States) and Quibt™ 2.0 fluorimeter (Thermo Fisher Scientific, Massachusetts, USA). We prepared DNA samples for sequencing on an Illumina HiSeq™ platform (Illumina, California, USA), generating 125+125bp paired-end sequencing using the Illumina HiSeq™ high output V4 chemistry. Isolates CLFT061, CLFT065, CLFT067, CLFT071, CLFT136 and CLFT144 were prepared using Illumina Nextera™ XT kits.

Autosomal read mapping and variant calling

All raw sequencing reads obtained from this study and from the previous studies were first cleaned of adapter sequences and quality trimmed using cutadapt v1.10 (*45*). Reads were mapped to the JEL423 reference genome (*23*) using Burrows-Wheeler Aligner (*46*) (BWA) v0.7.8. Resulting sequence alignment/map (SAM) files were processed using SAMtools (*47*) v1.3.1 using the 'fixmate' and 'sort' programs to ready the files for variant discovery. Variant discovery was performed in a two-step process using freebayes (*48*) version dbb6160 assuming a diploid genome in all individuals for the purposes of downstream analyses. Tests for the effect of ploidy variation on population genetic statistics in this study showed minimal bias due to this assumption (see online content methods section *Population structure and genomics analysis* for details). In the first step, sorted BAM files for each of the isolates in the study were independently called to find variant positions. The set of all variable positions identified across all samples were merged into a single variant call format (VCF)

file. In the second step, genotype calls were independently made for each isolate, at each of the positions identified in the first step to produce a squared-off call set (each sample VCF has genotype calls at the same loci, including homozygous reference calls, and explicitly identifying positions without sequencing read coverage). The sample VCF files were processed by *vcflib* (*49*) to break complex variants into allelic primitives and then vt (*50*) to normalize short insertion and deletion sequences (indels). VCFs were then quality filtered with *bcftools* (*47*) version 1.3.1. In individuals, sites covered by 3 reads or less were set to missing to ensure very low coverage sites did not contribute information. Subsequently, putative non-reference genotype calls were set to homozygous reference if they failed any of the following filters (there was not enough evidence to support a variant genotype call); an alternate allele is in the called genotype without supporting reads (AC > 0 && NUMALT == 0); the phred-scaled quality score is less than 5 when there are any reads covering the position (%QUAL < 5 && DP > 0); any called allele is not supported by at least two reads (AF[*] <= 0.5 && DP < 4); alternate alleles are supported by only low quality reads (AF[*] <= 0.5 && DP < 13 && %QUAL < 10) | (AF[*] > 0.5 && DP < 4 && %QUAL < 50); the quality, scaled by depth of supporting reads is less than a threshold (%QUAL / AO < 10); a called allele does not appear on both forward and reverse strands (SAF == 0 | SAR == 0); alleles are supported only by reads entirely placed right or left of the query variant (RPR = 0 | RPL = 0). The individual filtered VCF files were merged into a single multi-sample VCF using *vcfstreamsort* (*49*) to ensure sorting of out of order variants resulting from breaking complex variants in individual files into their simplest allelic representation.

Phylogenetic analysis, evolutionary rates and TMRCA for the amphibian panzootic

Positions including putative indels, and other complex and small structural variants were removed from the VCF leaving SNP positions only to maintain the alignment between sites. A FASTA file of the concatenated SNPs was constructed from these positions. Phylogenetic analyses were conducted using RAxML (*51*) v8.2.9 using the GTRCAT model with 500 bootstrap runs in rapid bootstrapping mode. A browsable version of this phylogeny with associated isolate metadata is

available on the microreact website (*19*) at https://microreact.org/project/GlobalBd. Mitochondrial reads were mapped to the JEL423 mitochondrial reference genomes and SNPs were called using the GATK UnifiedGenotyper (*52*) (v3.4-46-gbc0262) due to the haploid nature of the mitochondrial genome. A total of 1,150 high quality mitochondrial SNPs were called in the mitochondrial genome. Among those variants, 412, 194, 94 and 86 SNPs were contained within the *Bd*ASIA-1 (*n* = 8), *Bd*CAPE (*n* = 15), *Bd*GPL (*n* = 153) and *Bd*ASIA-2/*Bd*BRAZIL (*n* = 7) lineages respectively.

A non-recombining 1.66Mbp region from Supercontig_1.2 between positions 500,000-2,160,000 was identified as suitable input for the dating analysis from the autosomal genome. Owing to the highly dynamic organisation of the *Bd* genome (*18*) and subsequent rapid fluctuations in heterozygosity, and to scale the mutation rate by the number of variable and invariant sites, heterozygous SNPs in this region were 'haploidised' using a custom Perl script. A single allele at each site for each sample was selected using a weighted random-draw from the alleles observed at each locus, with weights equal to the sum of sequenced base qualities of the observed reads supporting each allele observed in the sequencing data (and not only from called genotypes, which are dependent on assumed ploidy). A ML phylogenetic tree was inferred with PhyML (*53*), using the haploidised and mitochondrial alignments, both of which recapitulate the whole-genome autosomal phylogeny.

Bayesian dating inferences were performed with BEAST (*54*) (v1.8.2) on 153 *Bd*GPL isolates with recorded sampling years. Isolate 0739 (*Bd*CH) was included as an outgroup in the phylogenetic reconstruction to improve the efficiency of tree search. We applied a GTR substitution model because the latter was shown using ModelTest (*55*) to best fit the SNP data. The xml input files were manually edited by adding the counts of invariant A, T, C & G sites as explained in Rieux & Balloux, Molecular Ecology, 2016 (see supplementary material 1a) (56). Rate variation among sites was modelled with a discrete gamma distribution with four rate categories. We assumed an uncorrelated lognormal relaxed clock to account for rate variation among lineages. To minimize prior assumptions about demographic history, we adopted an extended Bayesian skyline plot (EBSP) approach to integrate data over different coalescent histories.

The mitochondrial *Bd*GPL tree was calibrated using tip dates. To validate the tip dating additional calibration also using node dates (mixed calibration) was carried out. The autosomal

genome was calibrated using tip dates only. For tip dating inferences, we applied flat priors (i.e., uniform distributions) for the substitution rate (1.10^{-12} - 1.10^{-2} substitutions/site/year) as well as for the age of any node in the tree (including the root). For inference including node dating, we also applied the same flat prior for the substitution rate but we constrained the age of the MRCAs for Australian (1978) (4), Central American (1972) (5), Sierra de Guadarrama (1997) (*10*) and the Pyrenean (2000) (*57*) isolates to date to their respective historical description times. We used normal distributions as priors on nodal ages with the mean being equal to the historical description and a standard deviation of 20% the value of the mean. We initially ran an analysis, sampling from priors only to check the induced marginal prior distribution of the constrained nodes. The marginal priors of date-constrained nodes adequately matched the calibration densities we specified and there was no systematic bias in shifts away from the mean of the calibration densities (Fig S9). We ran a minimum of five independent chains in which samples were drawn every 10,000 MCMC steps from a total of 100,000,000 steps, after a discarded burn in of 10,000,000 steps. Convergence to the stationary distribution and sufficient sampling and mixing were checked by inspection of posterior samples (effective sample size >200). Parameter estimation was based on the samples combined from the different chains. The best supported tree was estimated from the combined samples using the maximum clade credibility method implemented in TreeAnnotator (*54*).

Targeted capture of Bd DNA from preserved amphibians specimens using RNA baits

The extraction, preparation, bait-enrichment and sequencing of *Batrachochytrium dendrobatidis* DNA preserved on amphibian skin was performed in a controlled environment in specialised ancient DNA laboratories at the Centre for GeoGenetics, Natural History Museum of Denmark. Amphibians from the Pyrenean *Bd* outbreak, -including the Pyrenean index site of Peñalara- were stored in 70% ethanol. Tissue (toe clips and ventral skin scrapes) was aseptically removed in a laminar flow hood and DNA was extracted using a Qiagen DNEasy™ Blood and Tissue kit (Qiagen, Venlo, Netherlands). DNA was sheared using sonication on a Biorupter™ (Diagenode, Liege, Belgium) using 6 cycles of 15 seconds on, followed by 90 seconds off to obtain 350-400bp fragments. Libraries

were prepared according to the blunt-end library preparation for degraded DNA described by Wales et al (*58*). Nicks in ligated adaptor sequences were repaired using a NEBNext™ fill-in module. Libraries were PCR amplified and P7 adaptor ends added using primers with custom barcode indexes. Samples underwent as few rounds of PCR as possible to minimise PCR amplification bias, using 12 cycles of PCR amplification with AmpliTaq Gold (Thermo Fisher Scientific, Massachusetts, USA). Indexed libraries were purified into 51ml *d*dH_20 using a Qiagen Qiaquick™ PCR purification kit. 300ng of each indexed library was enriched for *Batrachochytrium dendrobatidis* sequences using a custom-designed Mybaits™ kit (MYcroarray, Michigan, USA). RNA probes with a length of 120-mer were synthesized for the entire genome, using a 40 bp tiling strategy. The manufacture's recommended protocol was followed (Mybaits manual 1.3.8), including hybridisation of DNA and probes at 65℃ for 41 hours, and releasing the captured DNA from the RNA probes with an 10mM NaOH solution. Captured libraries were re-amplified with AmpliTaq Gold using 14 PCR cycles, inspected on a Bioanalyzer™ instrument (Agilent, California, USA) and sequenced on an Illumina HiSeq™ 2500 using paired end chemistry. Sequencing was carried out on captured libraries only. Reads were processed using the PALEOMIX (*59*) pipeline to produce BAM files for use in variant calling pipelines as described.

Resolving the structure of mtDNA using long-read sequencing

DNA from freshly cultured *Bd* reference isolate JEL423 (*23*) was carefully extracted using Qiagen Genomic Tips 20/G and DNeasy™ Blood and Tissue Kits (Qiagen, Venlo, Netherlands). DNA was size selected for high molecular weight (HMW) fragments using a QIAquick™ Gel Extraction Kit (Qiagen, Venlo, Netherlands). Size-selected DNA was subsequently sheared using Covaris g-tubes, preferentially shearing to obtain fragments of approximately 10 kbp. Libraries were prepared for long-read sequencing on a MinION™ sequencing device (Oxford Nanopore Technologies, Oxford, UK) using the Nanopore Sequencing Kit SQK-LSK208 (Oxford Nanopore Technologies, Oxford, UK). Libraries were run on a SpotON™ Flow Cell R9.4 (Oxford Nanopore Technologies, Oxford, UK) using a 48-hour run protocol.

Canu (*60*) was used to assemble resultant long reads, producing 4 unitigs. Using these unitigs as independent reference sequences, the long reads were re-mapped using Graphmap (*61*). Reads that mapped were extracted and reassembled using Canu. This improved (lengthened) the inverted repeat assembly at the termini of unitig2 and unitig4. The original Canu assembly produced longer inverted repeats for unitig1 and unitig3. The unitig variant with the longest terminal inverted repeat structure was selected for each of the 4 unitigs and combined into a single file. Previously sequenced Illumina HiSeq reads were mapped to the new long-read reference and Pilon (*62*) was used to improve the sequence assembly across 3 iterations. Based on contig overlap and coverage data the 4 unitigs were resolved into three mitochondrial chromosomes: unitig2-unitig1, unitig2-unitig3 and unitig4. Annotation was done using MFannot (*63*), InterProScan (*64*) for protein functional prediction and tRNAscan-SE(*65, 66*) to improve the tRNA predictions. Ribosomal RNA annotation was improved using the mapping of RNA-seq reads with accession number SRR3707957 (see Supplementary Materials Fig S7).

Population structure and genomics analysis

Sliding-window population genetic statistics (π, Tajima's D, F_{ST}) were calculated using vcftools (*67*) (v0.1.14) using 10kb non-overlapping windows. The ploidy of *Bd* genome is known to be variable (*18*) which violates the assumption of a diploid state used in these statistics. We tested for changes in π due to an effect of unaccounted-for increased ploidy. We predicted the ploidy of three samples with variable depth of coverage (JEL423, KB45 and VOR3) using a method based on genotype likelihoods. Briefly, the likelihood of a certain ploidy is equal to the sum across all possible genotype likelihoods compatible with the tested ploidy, times the probability of the genotype itself. The latter is calculated assuming Hardy-Weinberg Equilibrium using an expected population allele frequency with a constant effective population size of 100,000. We assigned the most likely ploidy at each supercontig as the most frequent ploidy across windows of 100kbp.

We then performed 10 simulations using 1Mbp segments from these isolates, where the ploidy was estimated to be equal to 3, 4 or 5. These segments of varying ploidy were then transformed to

diploids by either (i) randomly sampling two alleles at each genotype and (ii) using a strategy that favours heterozygous states if two alleles are present. With the former strategy, the mean overestimation of π (in standardised bias units) ranges from 1.0037 to 1.0061, while on the latter approach it ranges from 1.084 to 1.23. When the true ploidy is 1, we observe a mean underestimation (in standardised bias units) of 0.97. We therefore concluded that variation in ploidy cannot account for the large variation in π between the main lineages.

To explore population structure and signatures of ancient recombination using our complete, dense sequencing data, we used fineSTRUCTURE (*68*), which identifies haplotypes in the data and 'paints' individuals as a combination of those haplotypes. We used the linked co-ancestry model which uses information from markers in linkage disequilibrium, and we phased our sequencing data using the read-aware phasing algorithm implemented in shapeit2 (*69*) using these phased files as input to fineSTRUCTURE.

We also investigated population structure and genetic exchange among main lineages using STRUCTURE (*29, 70*) for a subset of sites and isolates. We selected a panel of 61 isolates representing all main lineages, and those isolates putatively identified as hybrids (Fig. 1b). We subsampled positions from our multi-sample VCF at a constant rate to equal to 10,000/586,005 (the total number of segregating sites in the VCF) using *vcfrandomsample* from vcflib (*49*) to obtain a random selection of 9,905 bi-allelic sites for analysis. We used the linked admixture model, without assuming correct phasing information for each site. After a burn-in of 10,000 MCMC iterations we sampled the posterior distribution from 20,000 iterations of the model to obtain joint-assignment probabilities for the ancestral population of origin for each site in each isolate. We varied the number of ancestral populations k, calculating the rate of change in the log probability of the data (*71*) across multiple replicates at each k, which indicated $k=4$ best explained the genetic structure in the population, broadly agreeing with deeply diverged phylogenetic lineages. The variance between replicates indicated that the length of our burn in and subsequent run-time was long enough.

The clustering of the global isolate panel was also investigated using principal component analysis (PCA). SNPs that were in high linkage disequilibrium were pruned from the dataset using the SNPRelate (*72*) package version 1.10.2 in R (*73*) version 3.4.0. After pruning using a sliding-window

based analysis and an LD threshold of 0.125, 3,900 SNP positions remained which were analysed using SNPrelate and plotted with ggplot2 (*74*).

Tests of association between chytridiomycosis and Bd lineage

All *Bd* isolates were classified as chytridiomycosis positive or negative (Supplementary Materials Fig. S11). Positive classifications were assigned where *Bd* isolates were observed to have caused clinical signs of disease or death in the wild in either the adult or tadpole from which the isolates were obtained. We examined differences for all isolates with geographic coordinates in the first instance (n=228). We also examined the potential effect of oversampling isolates from some locations. Fisher's tests (two tailed, p=0.05) were used to test for differences in the proportion of isolates associated with chytridiomycosis among main *Bd* lineages, where isolates were grouped into their parental lineages: *Bd*ASIA (consisting of *Bd*ASIA-1, *Bd*ASIA-2 and *Bd*BRAZIL); *Bd*GPL and *Bd*CAPE. Other lineages detected (all HYBRIDs and *Bd*CH) were excluded due to small sample sizes. *Post-hoc* tests with false-discovery rate (FDR) correction for multiple comparisons were used to determine statistical significance of differences between lineage pairs and to calculate odds ratios (Supplementary Materials Table S5).

We also examined the potential effect of oversampling isolates from some locations within the dataset by rerunning the tests of association after excluding isolates according to three geographic distance thresholds: 1) exact same location (0km); 2) within 0.5km, and 3) within 1km. Site pairs within each of these distance thresholds were first identified, and the first isolate of each pair of the same *Bd* lineage when ordered by latitude was retained for analyses while the other geographic duplicates were removed.

Bd multi-lineage challenge experiments

Experimental assessment of host response to *Bd* isolates was done according and subject to ethical review at the Institute of Zoology (Zoological Society of London), under UK Home Office

licence PPL 80/2466 in accordance with the A(SP)A Act 1986 and following established protocols (*31*). Common toad (*Bufo bufo*) larvae (Gosner stage 24 (*72*)) hatched from 20 egg strings collected in the UK were randomly allocated into 1 of 5 experimental treatment groups in two separate experiments for challenge with a *Bd* isolate from the *Bd*GPL, *Bd*CAPE, *Bd*CH or *Bd*ASIA-1 main lineages, or the negative control group. Each treatment comprised 60 individuals (biological replicates).

Tadpoles in *Bd* challenge treatments were exposed to 8 doses (7,500-37,500: mean 20,625 ± std. dev. 9,542 active zoospores per exposure in liquid media) of *Bd* zoospores every 4 days. Zoospore counts and volume of media were standardized among isolates for each exposure. Tadpoles in the negative control treatment were exposed on the same schedule to an equivalent volume of sterile media used to culture isolates. The experiment was undertaken in a climate-controlled room (18 °C constant temperature) with a 12h/12h day/night light schedule. Tadpoles were kept in individual flasks in 140 ml of aged water which were rotated daily. Water changes took place twice a week, and animals were fed with 0.4 mL solution of 1g/100ml powdered Tetra tablets every two days.

DNA from the tissue samples (mouth parts in larval stage and feet in metamorphs) was extracted in PrepMan Ultra (Applied Biosystems, Foster City, CA, USA; Hyatt et al. 2007) and analysed for the presence of *Bd* using quantitative (real-time) polymerase chain reaction techniques (qPCR) described by Boyle et al (*76*), and employing the changes described by Kriger et al (*77*). Extractions were diluted 1:10 before qPCR amplification, performed in duplicate, with *Bd* genomic equivalent (GE) standards of 100, 10, 1 and 0.1 GE.

To assess the effects of the different main *Bd* lineages on infectivity and survivorship we used an analysis of covariance (ANCOVA) with *Bd* lineage (treatment) as factor and body mass at metamorphosis as a covariate. Body mass was log-transformed to meet expectations of normality. Survivorship was assessed using Cox proportional hazards regression with treatment group and animal weight as covariates. It has been shown that exposure to *Bd* can affect larval development (*78-80*) so we examined the effect of treatment on time to metamorphosis, using one-way analysis of variance (ANOVA). By default, the last day of the experiment was considered the day of completion of the metamorphosis for those individuals that did not metamorphose by the endpoint. We also tested

for differential effects on body mass using ANCOVA at: 1) metamorphosis, using time to metamorphosis as covariate, and 2) at the end of the experiment using mass at metamorphosis and time post-metamorphosis as covariates. Mass and time were normalised by log-transformation.

The susceptibility to infection and survivorship of previously uninfected metamorphosed toads was tested using animals from the same egg strings as the larval challenge experiment. The animals were housed individually in plastic boxes (120 x 80 x 70 mm) lined with moist paper towel, provided with PVC shelter and kept on shelves in a climate-controlled environment at 18 °C. Box positions on each shelf were rotated daily to ensure each animal had equal lighting conditions across the duration of the experiment. Toadlets were fed on hatchling crickets every two days. The animals were allocated to be treated with one of the same 4 *Bd* treatments or the control treatment. *Bd* exposure treatments comprised being exposed to five doses (10,000-36,000: mean 20,200 ± std. dev. 10,639, active zoospores per exposure in liquid media) of *Bd* zoospores every 4 days. Each treatment comprised 30 toadlets. One control animal which was inadvertently contaminated was excluded from the analysis. Individuals were weighed before the experiment with no difference among different treatment groups (ANOVA: $F(4, 145) = 0.178$, $p = 0.949$). After 22 days, the experiment was completed and all animals were re-weighed. We tested for effects of treatment group (*Bd* lineage) on infectivity using ANCOVA, and tested survivorship using Cox's proportional hazards regression. We used Fisher's Least Significant Difference (LSD) test to determine *post hoc* where differences amongst treatments occurred, adjusting for multiple comparisons using false discovery rate correction.

Rooting the global phylogeny using orthoMCL

To root the *Bd* phylogenetic tree using *Bsal* as an outgroup (as opposed to a midpoint root as used in Fig 1b), VCF's, GFF3 and coding sequence (CDS) FASTAs for each gene in an updated *Bd* JEL423 gene set (*23*) were compared to generate consensus gene sequences for 7 isolates representing the full range of known *Bd* lineages (*Bd*CH=0739, *Bd*CAPE=SA6e, *Bd*ASIA-1=KB347, *Bd*ASIA-2/*Bd*BRAZIL=CLFT001 and KB72, *Bd*GPL=JEL423 and IA043). SNPs were included, and single

alleles were randomly chosen from heterozygous position. In an iterative process, we checked for any previous assignments of heterozygosity, and when present, we used the same allele. Each gene was translated to amino acid sequences using the universal genetic code. The first reading frame found to translate without stop codons was used, or that with the least number of stops. Single copy orthologous protein sequences for the *Bd* isolates, *Bsal* and 2 other chytrids *Hp* and *Sp* (*23*) were merged into individual files. We retained files with nucleotide substitutions between the *Bd* isolates resulting in 8 informative orthologous proteins for alignment using Muscle v3.8.31. From the protein alignments, we then extracted the CDS sequences and reformatted the alignment in a codon context, and merged into a single FASTA file. We identified DCMut+I+G as the best-fitting model (Supplementary Materials Table S2) of protein evolution using Prottest (*81*) v3.4 from all-matrices and all-distributions. We then ran RAxML (*51*) v8.2.9 with 500 bootstrap runs in rapid bootstrapping mode to generate the final tree (Supplementary Materials Fig. S6). We did not specify an outgroup to RAxML, but rooted the resultant tree using the *Bsal* outgroup.

Use of ITS-1 as a diagnostic marker for Bd lineage

A 50µl PCR reaction mixture was prepared for each sample, containing 32.5µl of dH_2O, 5µl of deoxyribonucleotides (dNTPs) at 2mM in equal ratio, 5µl of 10x buffer, 1µl each of the forward universal fungal ITS primer SF1 and the reverse universal fungal ITS primer SR1 (*16*), 0.5µl of Taq enzyme and 5µl of DNA sample. Primers were diluted to 10mM and the dNTPs to 2mM prior to use. PCR amplification proceeds as follows: 95℃ for 2 minutes, then 35 repetitions of 95℃ for 30 seconds, followed by annealing at 50℃ for 30 seconds, then extension at 72℃ for 2 minutes. A final extension at 72℃ for 7 minutes was carried out before holding at 4℃. 10µl of PCR product was analysed via gel electrophoresis using agarose gel and the DNA visualizer SafeView with a Hind III λ ladder to confirm successful amplification. The ITS region was visualised as a band around 500bp in size. The remainder of the PCR product was reserved for Multilocus Sequence Typing (MLST). Samples that were not successfully amplified with the SF1/SR1 primer combination were put through a nested PCR assay (*16*). 2µl of the original PCR product from the SF1/SR1 assay was added to a

master mix containing 35.5µl dH2O, 5µl each of dNTPs at 2mM and 10x buffer, 1µl of each of the *Bd* specific forward primer Bd1a and the *Bd* specific reverse primer Bd2a and 0.5µl of Taq enzyme. 10µl of PCR product was analysed as above via gel electrophoresis. MLST was carried out in either duplicate or, where possible, triplicate on all samples which were shown by gel electrophoresis to have undergone successful amplification. The sequencing reactions were Sanger-sequenced by Imperial College London's MRC CSC Genomics Core Laboratory. The Sanger sequences were imported into CodonCode where low quality ends were trimmed and consensus sequences assigned using Phred base-calling. Sequences were aligned using Clustal–W in Mega (*82*) V.6 and a ML Tree, with 500 bootstrap replications was computed (Supplementary Materials Fig. S3).

Additional R packages used

Additional R (*73*) packages used for generating figures include; *ggplot2* (*74)*, *RColorBrewer* (*88,89*), *data.table* (*90*), *ggtree* (*91*), *dendextend* (*92*) and *ape* (*93*).

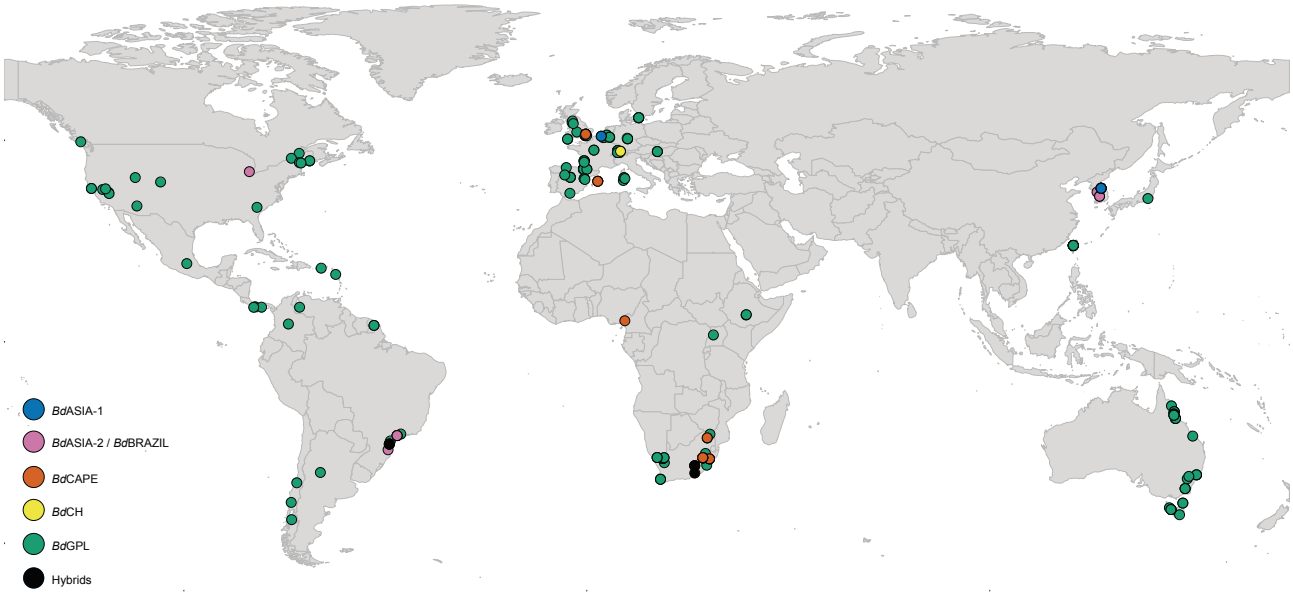

Fig. S1.
Isolate sampling locations. Sampling points are coloured by lineage.

Caption for Fig. S2

Available online as a PDF file. Nuclear phylogeny. A phylogeny was constructed from the 586,005 segregating sites in the nuclear genome using the GTRCAT substitution model implemented in RAxML. Five hundred bootstrap replicates were performed. The phylogeny is mid-point rooted.

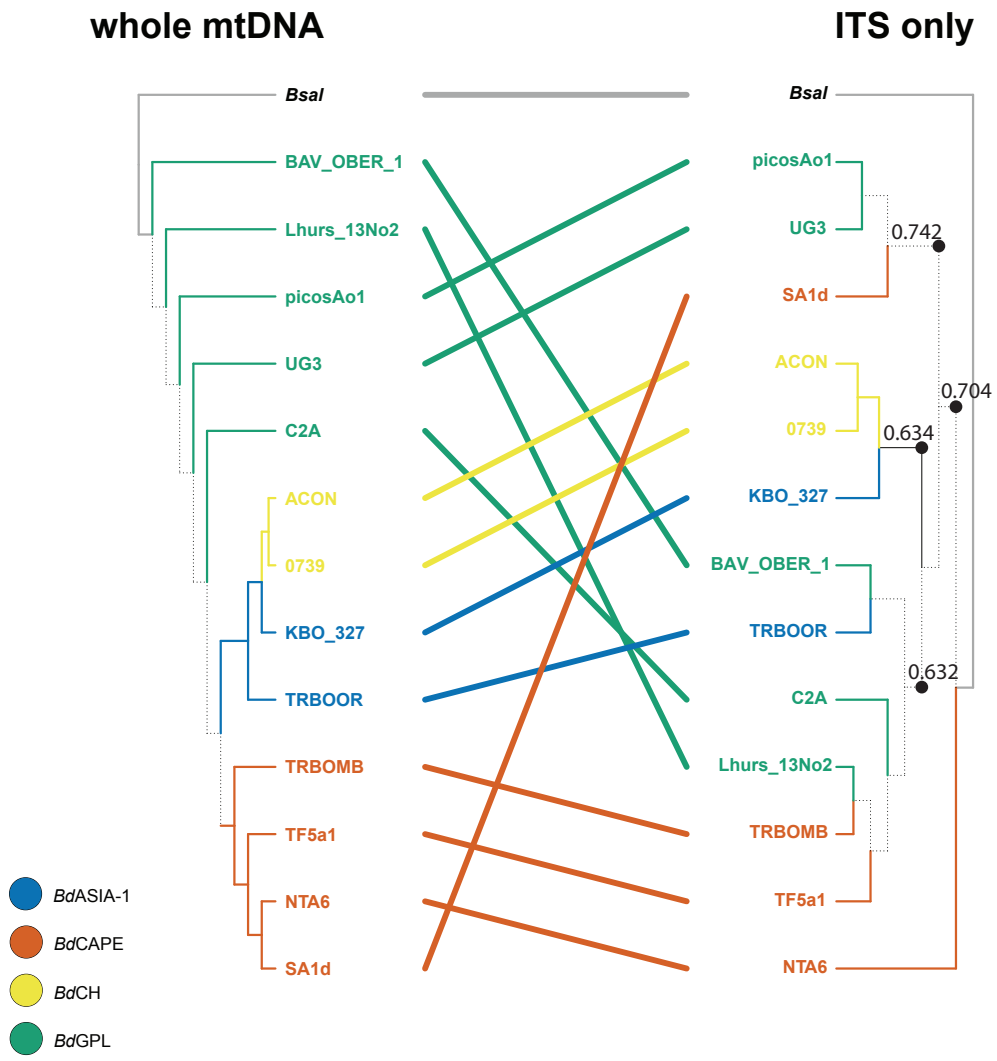

Fig. S3

Comparison of phylogenies generated from mitochondrial and internal transcribed spacer (ITS) sequence alignments. Phylogenetic trees generated from mitochondrial alignments recapitulate the deeply diverged, main lineages obtained from whole nuclear genome alignments. ITS alignments are not able to distinguish main *Bd* lineage, grouping isolates from different lineages with high bootstrap support (high support values for ITS tree displayed at internal nodes labelled with black dots).

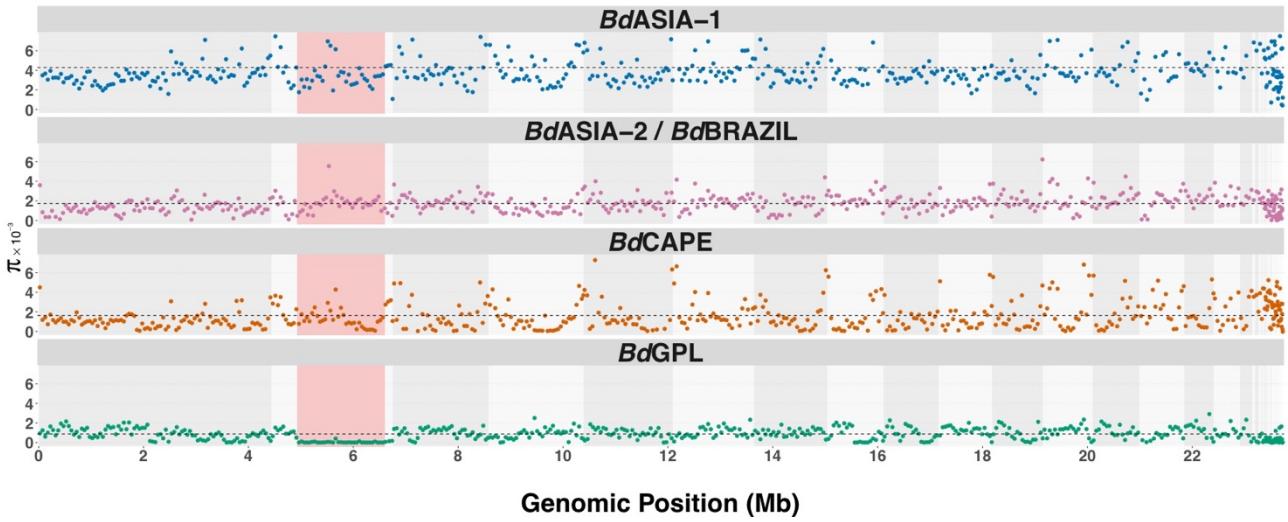

Fig. S4

Nulceotide diversity (π). A non-overlapping sliding window of 10kb width was used to calculate nucleotide diversity for each of the lineages. The region highlighted in red is the region of low-recombination identified in the *Bd*GPL lineage. The dashed black horizontal line in each panel denotes average π.

Caption for Fig. S5

Available online as a PDF file. fineSTRUCTURE analysis of haplotype sharing among lineages. The scale bar represents the amount of genomic sharing (number of haplotype chunks), with dark purple representing the largest number of shared haplotypes, and yellow representing the least number of shared haplotypes. The dendrogram at the top is coloured according to lineage.

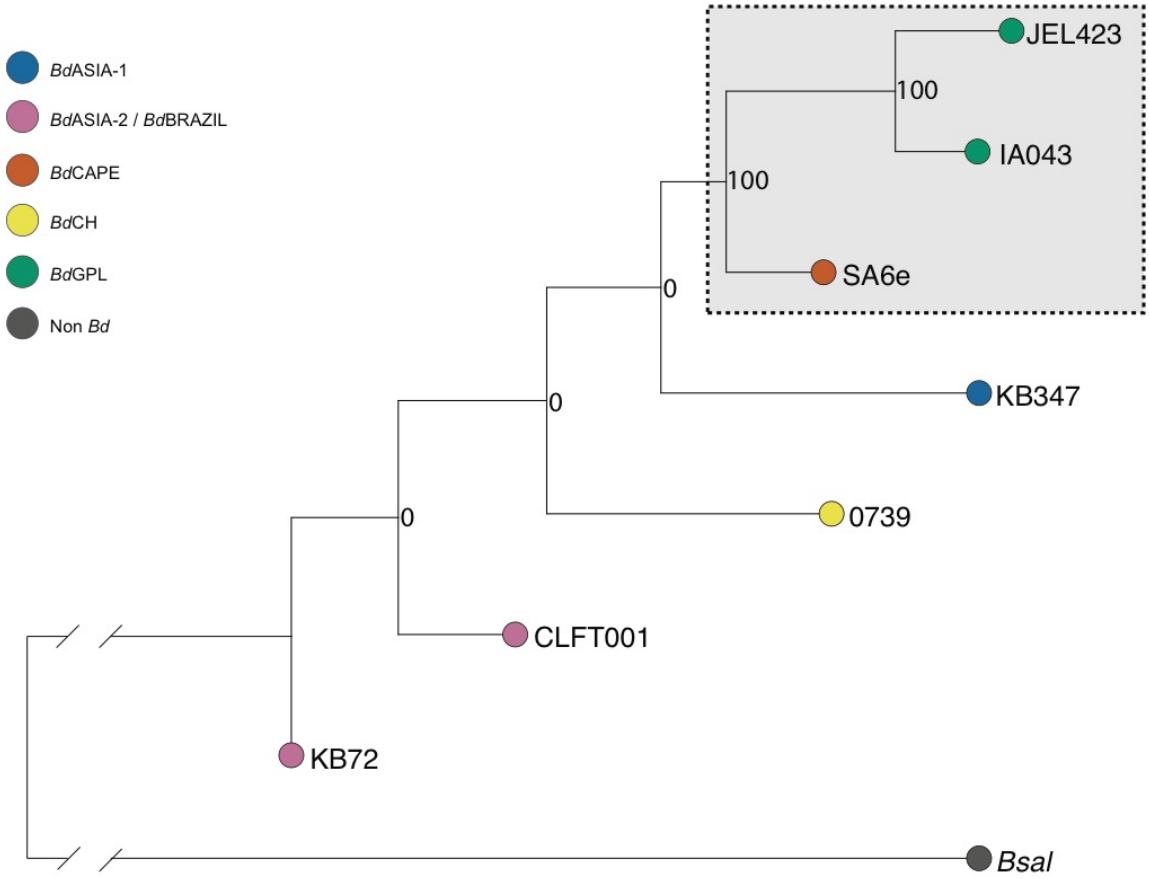

Fig. S6

A *Bd* phylogeny rooted with the outgroup *Batrachochytrium salamandrivorans* (*Bsal*). This phylogeny shows the inferred relationships among the four main lineages of *Bd*. The region of the phylogeny highlighted in grey, shows strongly supported internal branches, lending support to *Bd*CAPE and *Bd*GPL more different to *Bsal* than *Bd*ASIA-1 or *Bd*ASIA-2/*Bd*BRAZIL. The values on the phylogeny denote bootstrap support values from 1000 bootstrap replicates.

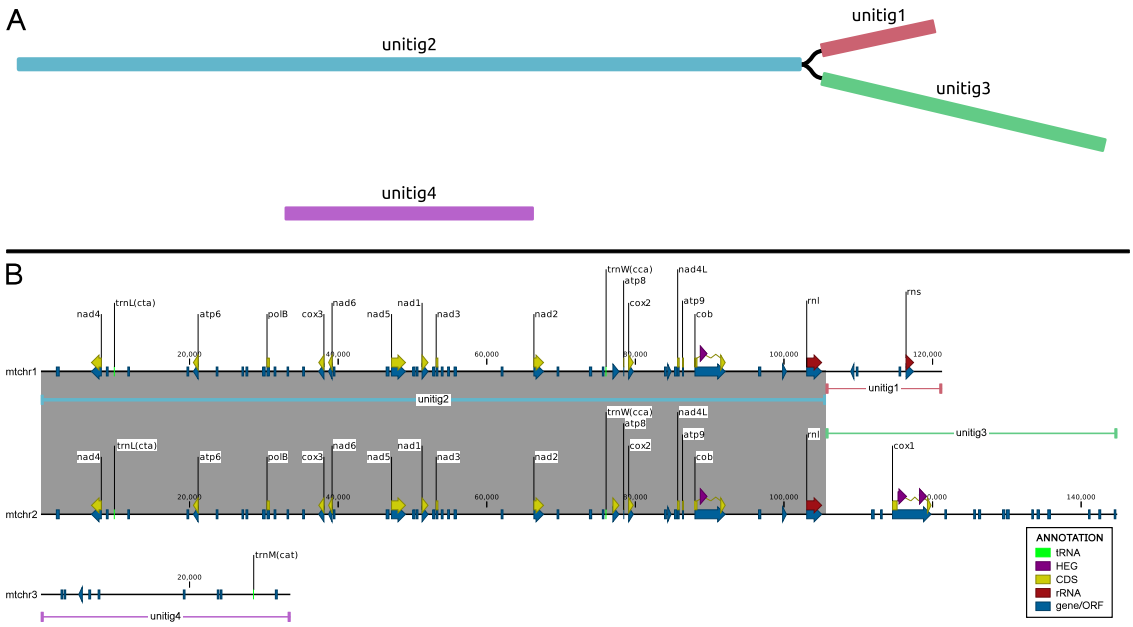

Fig. S7

Structure of *Bd* mtDNA resolved using long-read sequencing. a. Graph representation of the mitochondrial genome using Bandage (*83*). Canu assembly of the mitochondrial genome resulted in four unitigs that belong to three linear chromosomes that terminated in inverted repeats. b. Genetic map of the mitochondrial chromosomes and how they relate to the four unitigs. Grey region is the shared (homologous) region that corresponds to unitig2, which can be found in both large chromosomes. Unitig2 had twice as high coverage as the other mtDNA unitigs, and it was linked with unitig1 and unitig3 with equal support. Homology of the shared region is assumed to be maintained by recombination between the two chromosomes. Most of the conserved mitochondrial genes are located in the shared region except for *rns* (or mtSSU rRNA) and *cox1* (or COI). In addition, the shared region contains a tRNA gene recognizing UAG codon as leucine (typical for chytrid mtgenomes (*84*)) and DNA-polymerase (*polB*) that is associated with linear mitochondrial chromosomes terminating in inverted repeats(*85-87*). ORFs (open reading frames) lacking functional prediction are shown as blue arrows or boxes without tags. HEG stands for homing endonuclease gene (commonly associated with group I and II introns). CDS stands for coding sequence region of protein coding genes.

Caption for Fig. S8

Available online as a PDF file. Counts of heterozygous positions for each isolate plotted against a phylogeny. Counts were binned into 10kbp stretches of DNA and plotted against the midpoint rooted phylogeny depicted in Fig 1b. The red highlighted region is the identified low recombination region that shows a striking loss of heterozygosity across all isolates of *Bd*GPL. This same region exhibits no loss of heterozygosity at all in *Bd*ASIA-1.

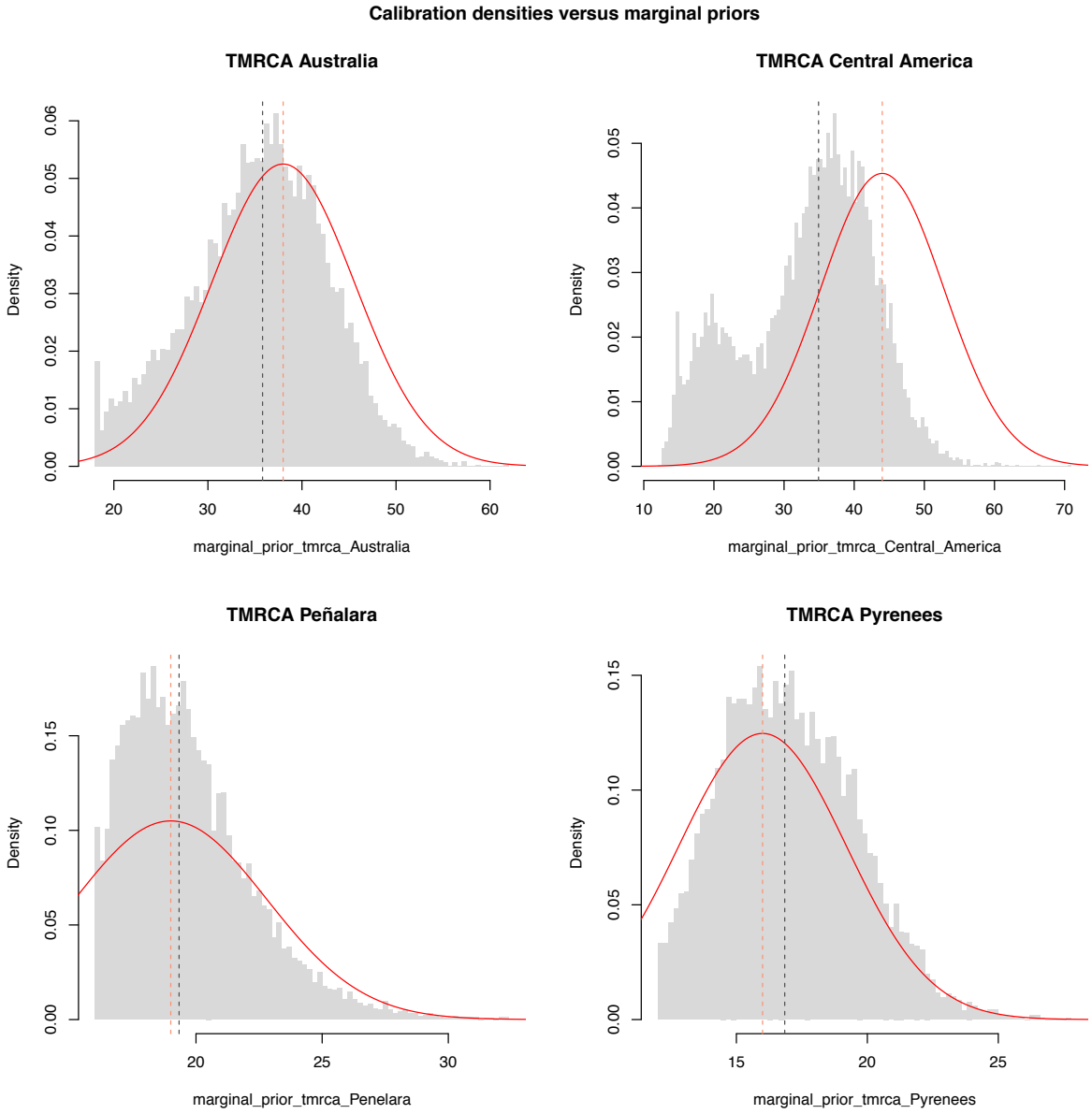

Fig. S9

Histogram of marginal priors (grey) for each of the constrained nodes in the mixed dating analysis in BEAST. The specified (normally distributed) calibration densities for each node are overlaid in red. The mean of the calibration densities is denoted by the red vertical line. The median of each marginal prior distribution is denoted by the vertical black lines.

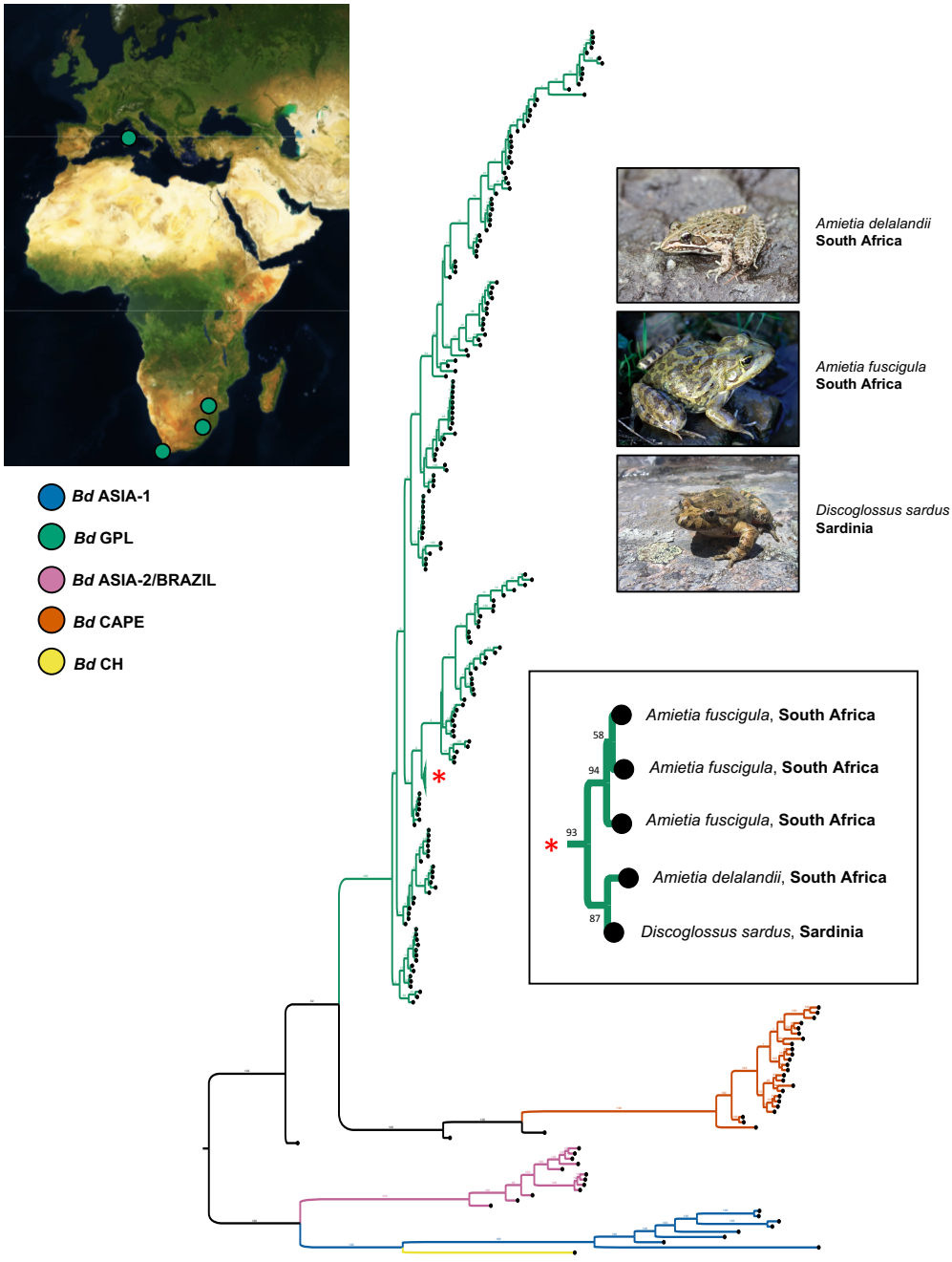

Fig. S10

Transcontinental clusters of infection amongst isolates of *Bd*GPL showing international linkages with high (>90%) bootstrap support. In this example, isolates of *Bd* recovered from *Discoglossus sardus* on the Mediterranean island of Sardinia are closely linked to isolates of *Bd* recovered from species of *Amietia* from South Africa. A browsable version of this phylogeny can be accessed at https://microreact.org/project/GlobalBd

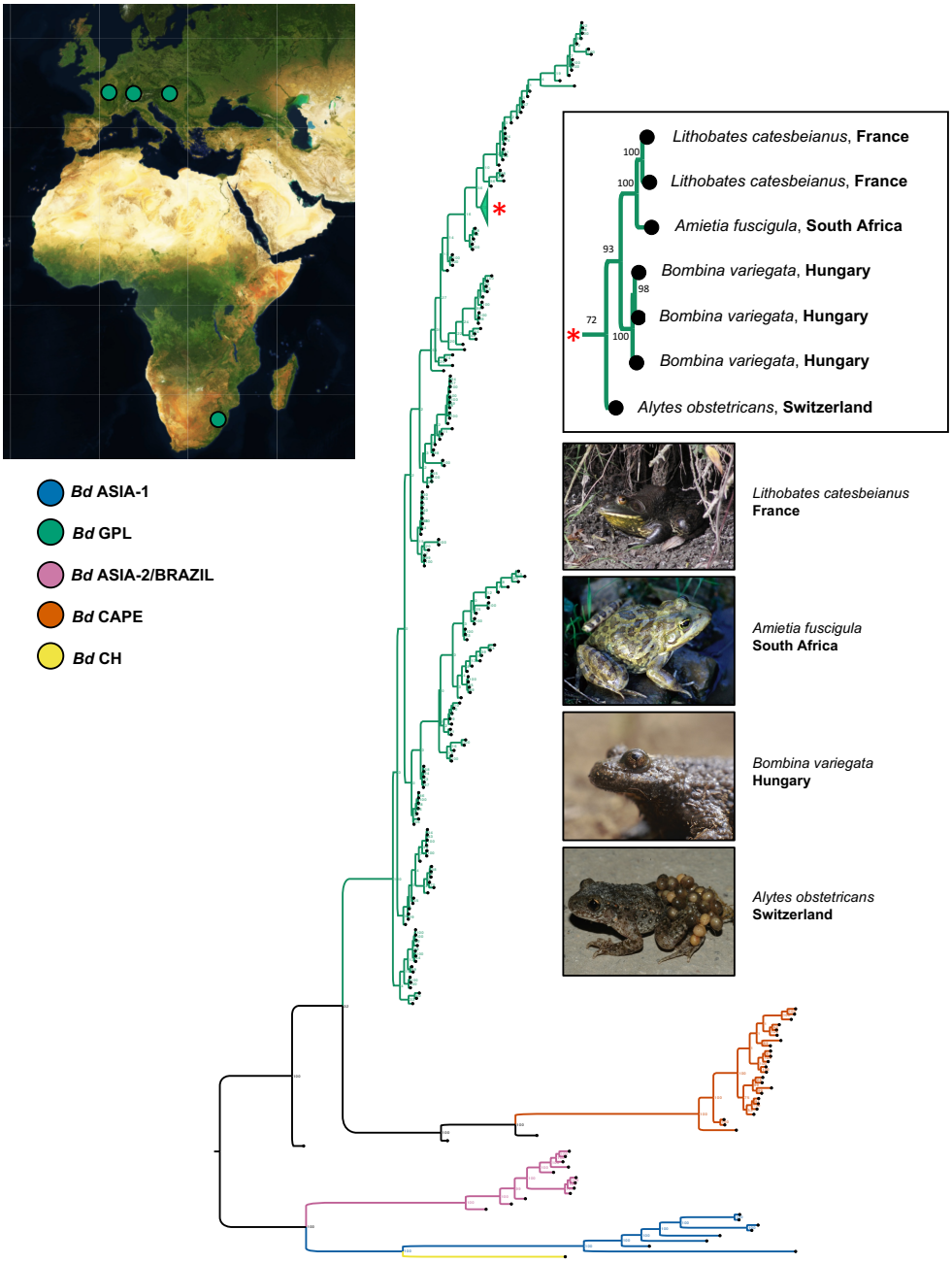

Fig. S11

Transcontinental clusters of infection amongst isolates of *Bd*GPL showing international linkages with high (>90%) bootstrap support. In this example, isolates of *Bd* recovered invasive non-native North American bullfrogs in France and fire-bellied toads from Hungary are closely linked to an isolate of *Bd* recovered from *Amietia fuscigula* from South Africa. A browsable version of this phylogeny can be accessed at https://microreact.org/project/GlobalBd

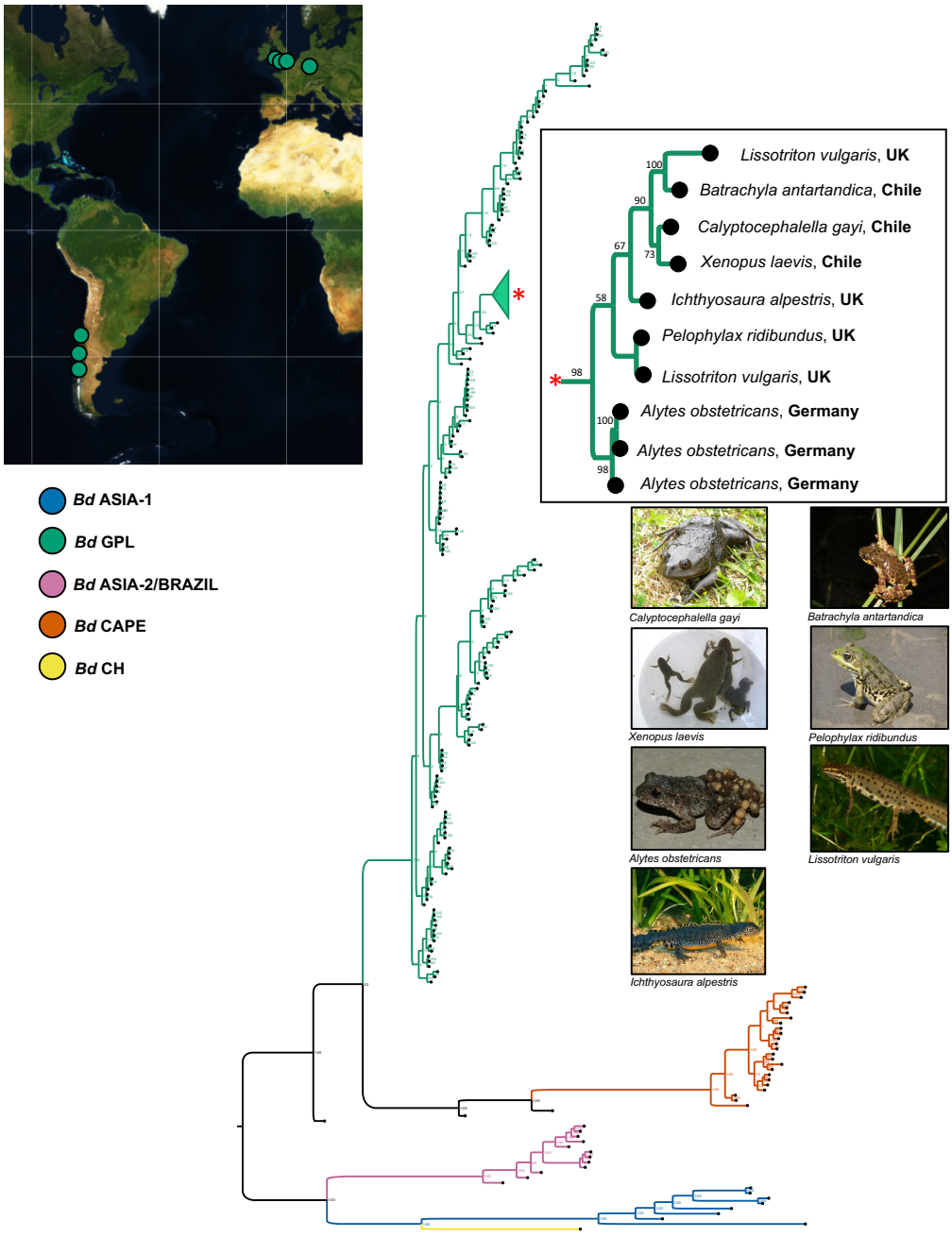

Fig. S12

Transcontinental clusters of infection amongst isolates of *Bd*GPL showing international linkages with high (>90%) bootstrap support. In this example, isolates of *Bd* recovered native and non-native species of amphibian in Chile are closely linked to isolates of *Bd* recovered from species of amphibians across Europe. A browsable version of this phylogeny can be accessed at https://microreact.org/project/GlobalBd

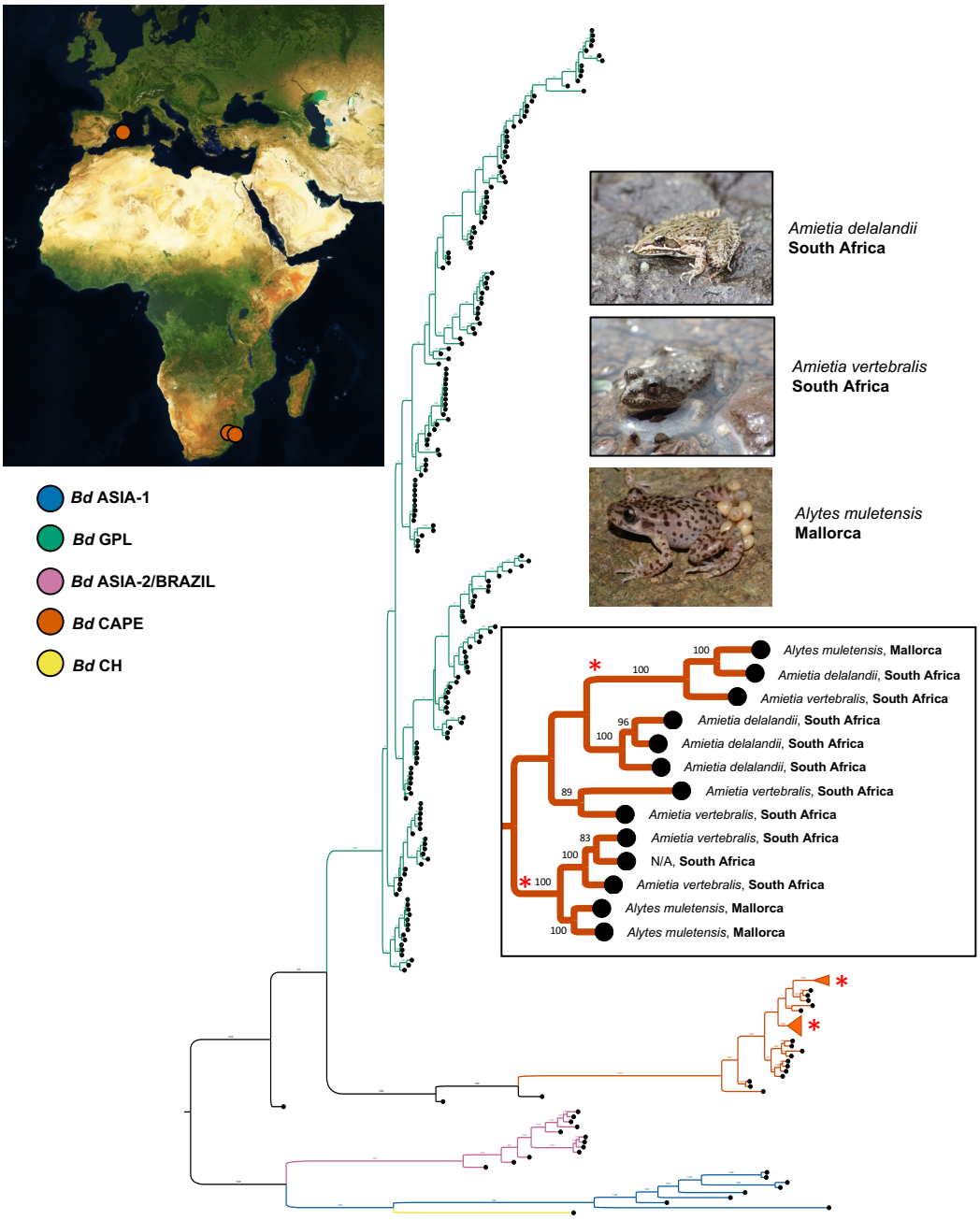

Fig. S13

Transcontinental clusters of infection amongst isolates of *Bd*CAPE showing international linkages with high (>90%) bootstrap support. In this example, isolates of *Bd* from Mallorcan midwife toads are closely linked to isolates of *Bd* recovered amphibians in South Africa, confirming the hypothesis by Walker *et al.* Current Biology 2008 (*35*). A browsable version of this phylogeny can be accessed at https://microreact.org/project/GlobalBd

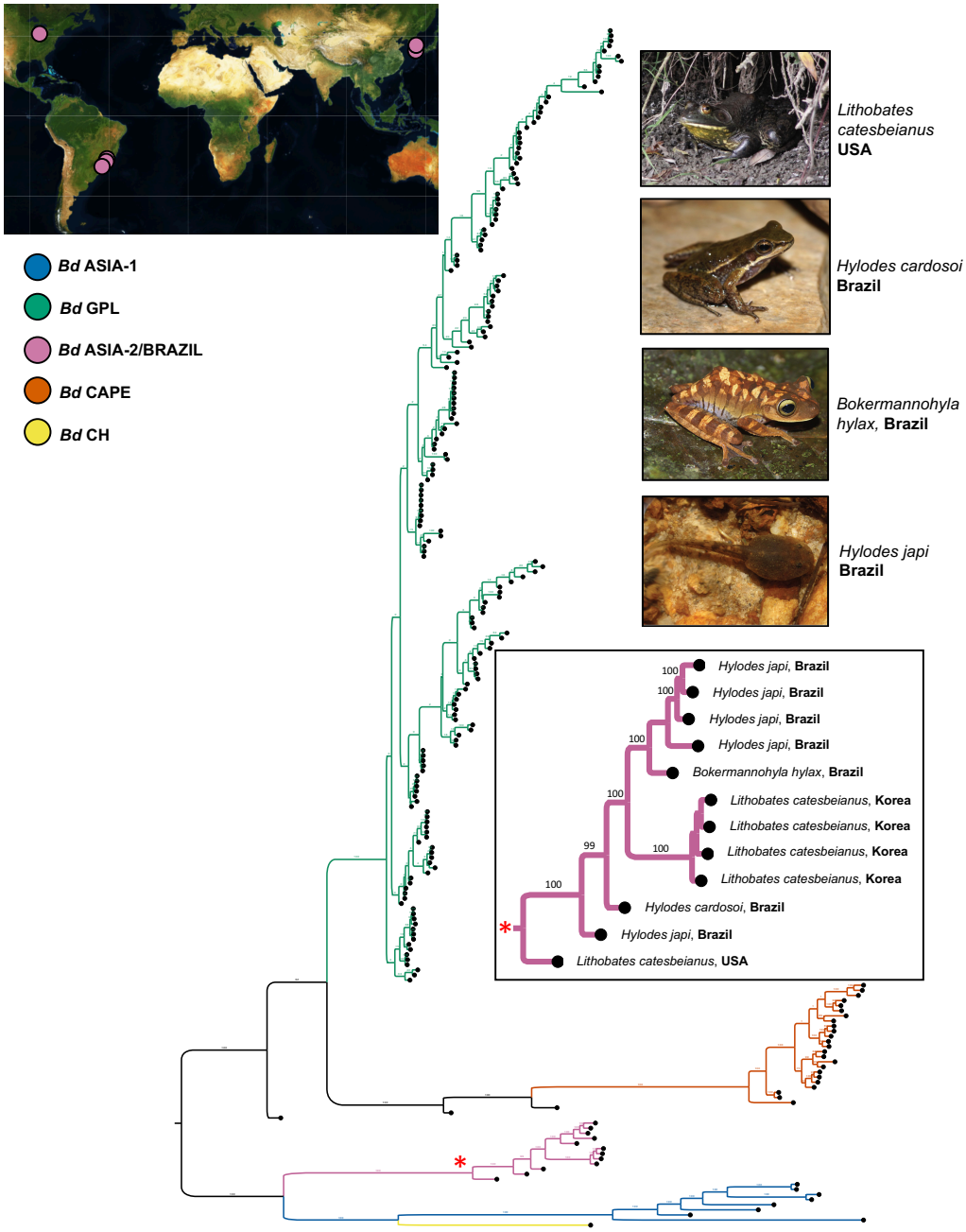

Fig. S14

Transcontinental clusters of infection amongst isolates of *Bd*ASIA-2/*Bd*Brazil showing international linkages with high (>90%) bootstrap support. In this example, isolates of *Bd* from North American bullfrogs in South Korea are closely linked to isolates recovered from amphibians in Brazil. A browsable version of this phylogeny can be accessed at https://microreact.org/project/GlobalBd

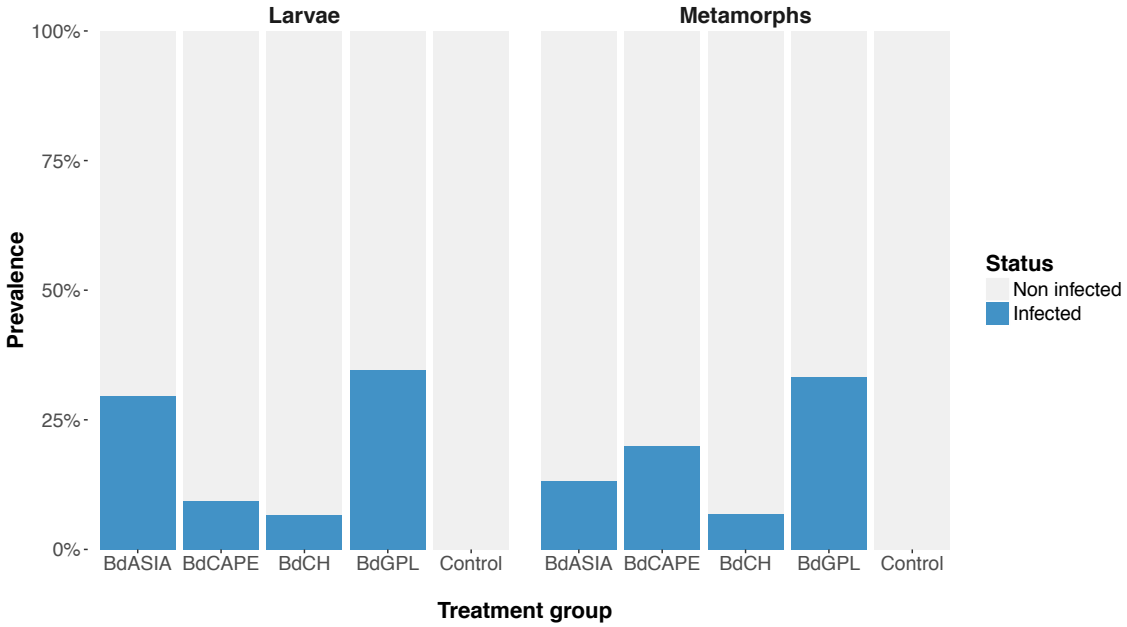

Fig. S15

Prevalence of *Bd* infection after exposure to different lineages during larval stage and early terrestrial stage.

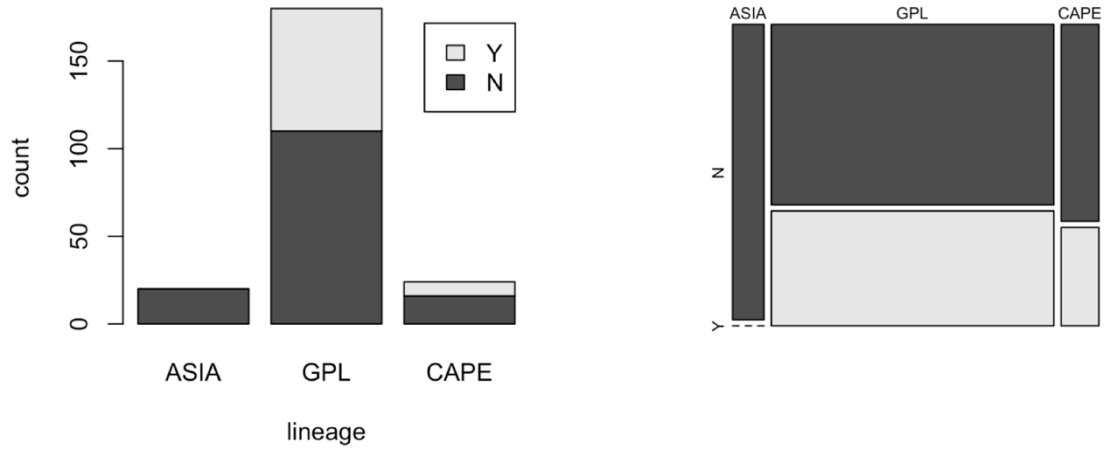

Fig. S16

Association between chytridiomycosis and main *Bd* lineages. The *Bd*ASIA-1 and *Bd*ASIA-2/BRAZIL lineages were grouped into a single assumed parental lineage (labelled ASIA). The bar chart of the left gives counts of cases and non-cases of chytridiomycosis for each of the lineages. The plot on the right gives the relative proportion for each of the lineages. Asian and endemic Brazilian strains were not associated with any cases of chytridiomycosis.

Caption for Table S1

Available online as an Excel file. Metadata associated with isolates used in this study.

Table S2

Likelihood for different models of protein evolution fit to *Bd*/*Bsal* protein alignments in *Prottest v3.4*.

Model	deltaLnL	LnL	LnLw	-lnL
DCMut+I+G	0	12773033.24	1	12773033.24
Dayhoff+I+G	737.1	12773770.34	0	12773770.34
DCMut+G	14986.51	12788019.75	0	12788019.75
Dayhoff+G	15702.76	12788736	0	12788736
DCMut+I	32175.93	12805209.17	0	12805209.17
Dayhoff+I	32455.96	12805489.2	0	12805489.2
DCMut	316469.3	13089502.54	0	13089502.54
Dayhoff	318527.3	13091560.54	0	13091560.54
WAG+I	383916.71	13156949.94	0	13156949.94
WAG+I+G	383955.38	13156988.62	0	13156988.62
WAG+G	398459.69	13171492.93	0	13171492.93
WAG	514689.17	13287722.41	0	13287722.41
Blosum62+I+G	524054.62	13297087.86	0	13297087.86
Blosum62+I	524634.48	13297667.72	0	13297667.72
Blosum62+G	526363.77	13299397.01	0	13299397.01
Blosum62	579023.94	13352057.18	0	13352057.18
JTT+I	623633.02	13396666.26	0	13396666.26
JTT+I+G	623650.41	13396683.65	0	13396683.65
JTT+G	637497.91	13410531.15	0	13410531.15
JTT	770388.94	13543422.18	0	13543422.18
LG+I	978698.32	13751731.56	0	13751731.56
LG+I+G	978952.45	13751985.69	0	13751985.69
LG+G	996008.37	13769041.61	0	13769041.61
VT+I+G	1009335.06	13782368.3	0	13782368.3
VT+G	1025258.35	13798291.59	0	13798291.59
FLU+I+G	1034524.76	13807558	0	13807558

Table S3

Mean time to metamorphosis, mean mass at metamorphosis and percentage survival of individuals under the varied *Bd* lineage treatments. Mean time and mass are displayed ± the standard error.

Treatment (lineage)	Mean time to metamorphosis (days)	Mean mass at metamorphosis (g)	Survival (%)
Control	40.43 ± 0.706	0.102 ± 0.0025	91.4
*Bd*CAPE	39.29 ± 0.500	0.103 ± 0.0018	91.4
*Bd*ASIA-1	39.11 ± 0.521	0.098 ± 0.0019	80.6
*Bd*CH	42.63 ± 0.899	0.095 ± 0.0020	81.6
*Bd*GPL	40.80 ± 0.671	0.098 ± 0.0016	80.0

Table S4

Statistical tests for significant differences between treatment groups for *B. dendrobatidis* infection. Fisher's least significant difference ($p < 0.05$) with false discovery rate correction for multiple comparisons was used to determine significant differences between treatment group means for *B. dendrobatidis* prevalence for larval and post-metamorphic experiments. Statistical significance when p-value < 0.05.

Experiment #1 (Larval)				
Treatment (lineage)	***Bd*GPL**	***Bd*CAPE**	***Bd*CH**	***Bd*ASIA-1**
*Bd*CAPE	**< 0.01**			
*Bd*CH	**< 0.01**	0.621		
*Bd*ASIA-1	0.424	**< 0.01**	**< 0.01**	
Control	**< 0.01**	0.136	0.297	**< 0.01**
Experiment #2 (Metamorph)				
*Bd*CAPE	0.206			
*Bd*CH	**< 0.05**	0.206		
*Bd*ASIA-1	0.066	0.472	0.472	
Control	**< 0.01**	0.066	0.472	0.206

Table S5

Statistical tests for significant differences between *Bd* lineage and association with chytridiomycosis. Fisher's tests (two tailed, p=0.05) were used to test for differences in the proportion of isolates associated with chytridiomycosis among *Bd* lineages, where isolates were grouped into their parental lineages: ASIA (consisting of *Bd*ASIA-1, *Bd*ASIA-2 and *Bd*BRAZIL); CAPE and GPL. p values reported in main text were calculated using false discovery rate correction for multiple comparisons; Bonferroni corrected p values are also shown above.

Lineage	Lower 95% CI	Odds ratio	Upper 95% CI	Fisher's test *P*	False Discovery Rate *p*	Bonferroni corrected *p*
*Bd*ASIA vs *Bd*CAPE	1.760	Inf	Inf	0.0049	0.0073	0.0146
*Bd*ASIA vs *Bd*GPL	3.001	Inf	Inf	0.0001	0.0004	0.0004
*Bd*GPL vs *Bd*CAPE	0.276	0.787	2.072	0.6606	0.6606	1.0000

Dataset S1

Available online as a zipped xml file. BEAST settings and prior specifications used in the tip-based mitochondrial genome dating analysis

Dataset S2

Available online as a zipped xml file. BEAST settings and prior specifications used in the tip-based autosomal genome dating analysis

Dataset S3

Available online as a zipped xml file. BEAST settings and prior specifications used in the node and tip-based mitochondrial genome dating analysis

References

1. M. C. Fisher, D. A. Henk, C. J. Briggs, J. S. Brownstein, L. C. Madoff, S. L. McCraw, S. J. Gurr, Emerging fungal threats to animal, plant and ecosystem health. *Nature* **484**, 186–194 (2012). doi:10.1038/nature10947 Medline

2. L. Berger, R. Speare, P. Daszak, D. E. Green, A. A. Cunningham, C. L. Goggin, R. Slocombe, M. A. Ragan, A. D. Hyatt, K. R. McDonald, H. B. Hines, K. R. Lips, G. Marantelli, H. Parkes, Chytridiomycosis causes amphibian mortality associated with population declines in the rain forests of Australia and Central America. *Proc. Natl. Acad. Sci. U.S.A.* **95**, 9031–9036 (1998). doi:10.1073/pnas.95.15.9031 Medline

3. A. R. Blaustein, D. B. Wake, Declining amphibian populations: A global phenomenon? *Trends Ecol. Evol.* **5**, 203–204 (1990). doi:10.1016/0169-5347(90)90129-2

4. L. F. Skerratt, L. Berger, R. Speare, S. Cashins, K. R. McDonald, A. D. Phillott, H. B. Hines, N. Kenyon, Spread of chytridiomycosis has caused the rapid global decline and extinction of frogs. *EcoHealth* **4**, 125–134 (2007). doi:10.1007/s10393-007-0093-5

5. T. L. Cheng, S. M. Rovito, D. B. Wake, V. T. Vredenburg, Coincident mass extirpation of neotropical amphibians with the emergence of the infectious fungal pathogen *Batrachochytrium dendrobatidis*. *Proc. Natl. Acad. Sci. U.S.A.* **108**, 9502–9507 (2011). doi:10.1073/pnas.1105538108 Medline

6. K. R. Lips, J. Diffendorfer, J. R. Mendelson, M. W. Sears, Riding the wave: Reconciling the roles of disease and climate change in amphibian declines. *PLOS Biol.* **6**, e72 (2008). doi:10.1371/journal.pbio.0060072 Medline

7. T. Carvalho, C. G. Becker, L. F. Toledo, Historical amphibian declines and extinctions in Brazil linked to chytridiomycosis. *Proc. R. Soc. B* **284**, 20162254 (2017). doi:10.1098/rspb.2016.2254 Medline

8. M. A. Hudson, R. P. Young, J. D. Jackson, P. Orozco-terWengel, L. Martin, A. James, M. Sulton, G. Garcia, R. A. Griffiths, R. Thomas, C. Magin, M. W. Bruford, A. A. Cunningham, Dynamics and genetics of a disease-driven species decline to near extinction: Lessons for conservation. *Sci. Rep.* **6**, 30772 (2016). doi:10.1038/srep30772

9. L. J. Rachowicz, R. A. Knapp, J. A. T. Morgan, M. J. Stice, V. T. Vredenburg, J. M. Parker, C. J. Briggs, Emerging infectious disease as a proximate cause of amphibian mass mortality. *Ecology* **87**, 1671–1683 (2006). doi:10.1890/0012-9658(2006)87[1671:EIDAAP]2.0.CO;2 Medline

10. J. Bosch, I. Martinez-Solano, M. Garcia-Paris, Evidence of a chytrid fungus infection involved in the decline of the common midwife toad (*Alytes obstetricans*) in protected areas of central Spain. *Biol. Conserv.* **97**, 331–337 (2001). doi:10.1016/S0006-3207(00)00132-4

11. R. A. Farrer, L. A. Weinert, J. Bielby, T. W. J. Garner, F. Balloux, F. Clare, J. Bosch, A. A. Cunningham, C. Weldon, L. H. du Preez, L. Anderson, S. L. K. Pond, R. Shahar-Golan, D. A. Henk, M. C. Fisher, Multiple emergences of genetically diverse amphibian-infecting chytrids include a globalized hypervirulent recombinant lineage. *Proc. Natl. Acad. Sci. U.S.A.* **108**, 18732–18736 (2011). doi:10.1073/pnas.1111915108 Medline

12. E. B. Rosenblum, T. Y. James, K. R. Zamudio, T. J. Poorten, D. Ilut, D. Rodriguez, J. M. Eastman, K. Richards-Hrdlicka, S. Joneson, T. S. Jenkinson, J. E. Longcore, G. Parra Olea, L. F. Toledo, M. L. Arellano, E. M. Medina, S. Restrepo, S. V. Flechas, L. Berger, C. J. Briggs, J. E. Stajich, Complex history of the amphibian-killing chytrid fungus revealed with genome resequencing data. *Proc. Natl. Acad. Sci. U.S.A.* **110**, 9385–9390 (2013). doi:10.1073/pnas.1300130110 Medline

13. C. Weldon, L. H. du Preez, A. D. Hyatt, R. Muller, R. Spears, Origin of the amphibian chytrid fungus. *Emerg. Infect. Dis.* **10**, 2100–2105 (2004). doi:10.3201/eid1012.030804 Medline

14. B. L. Talley, C. R. Muletz, V. T. Vredenburg, R. C. Fleischer, K. R. Lips, A century of *Batrachochytrium dendrobatidis* in Illinois amphibians (1888-1989). *Biol. Conserv.* **182**, 254–261 (2015). doi:10.1016/j.biocon.2014.12.007

15. D. Rodriguez, C. G. Becker, N. C. Pupin, C. F. B. Haddad, K. R. Zamudio, Long-term endemism of two highly divergent lineages of the amphibian-killing fungus in the Atlantic Forest of Brazil. *Mol. Ecol.* **23**, 774–787 (2014). doi:10.1111/mec.12615 Medline

16. K. Goka, J. Yokoyama, Y. Une, T. Kuroki, K. Suzuki, M. Nakahara, A. Kobayashi, S. Inaba, T. Mizutani, A. D. Hyatt, Amphibian chytridiomycosis in Japan: Distribution, haplotypes and possible route of entry into Japan. *Mol. Ecol.* **18**, 4757–4774 (2009). doi:10.1111/j.1365-294X.2009.04384.x Medline

17. A. Bataille, J. J. Fong, M. Cha, G. O. U. Wogan, H. J. Baek, H. Lee, M. S. Min, B. Waldman, Genetic evidence for a high diversity and wide distribution of endemic strains of the pathogenic chytrid fungus *Batrachochytrium dendrobatidis* in wild Asian amphibians. *Mol. Ecol.* **22**, 4196–4209 (2013). doi:10.1111/mec.12385 Medline

18. R. A. Farrer, D. A. Henk, T. W. J. Garner, F. Balloux, D. C. Woodhams, M. C. Fisher, Chromosomal copy number variation, selection and uneven rates of recombination reveal cryptic genome diversity linked to pathogenicity. *PLOS Genet.* **9**, e1003703 (2013). doi:10.1371/journal.pgen.1003703 Medline

19. S. Argimón, K. Abudahab, R. J. E. Goater, A. Fedosejev, J. Bhai, C. Glasner, E. J. Feil, M. T. G. Holden, C. A. Yeats, H. Grundmann, B. G. Spratt, D. M. Aanensen, Microreact: Visualizing and sharing data for genomic epidemiology and phylogeography. *Microb. Genomics* **2**, e000093 (2016). doi:10.1099/mgen.0.000093 Medline

20. L. M. Schloegel, L. F. Toledo, J. E. Longcore, S. E. Greenspan, C. A. Vieira, M. Lee, S. Zhao, C. Wangen, C. M. Ferreira, M. Hipolito, A. J. Davies, C. A. Cuomo, P. Daszak, T. Y. James, Novel, panzootic and hybrid genotypes of amphibian chytridiomycosis associated with the bullfrog trade. *Mol. Ecol.* **21**, 5162–5177 (2012). doi:10.1111/j.1365-294X.2012.05710.x Medline

21. D. J. Lawson, G. Hellenthal, S. Myers, D. Falush, Inference of population structure using dense haplotype data. *PLOS Genet.* **8**, e1002453 (2012). doi:10.1371/journal.pgen.1002453 Medline

22. L. Li, C. J. Stoeckert Jr., D. S. Roos, OrthoMCL: Identification of ortholog groups for eukaryotic genomes. *Genome Res.* **13**, 2178–2189 (2003). doi:10.1101/gr.1224503 Medline

23. R. A. Farrer, A. Martel, E. Verbrugghe, A. Abouelleil, R. Ducatelle, J. E. Longcore, T. Y. James, F. Pasmans, M. C. Fisher, C. A. Cuomo, Genomic innovations linked to infection strategies across emerging pathogenic chytrid fungi. *Nat. Commun.* **8**, 14742 (2017). doi:10.1038/ncomms14742 Medline

24. F. Tajima, Statistical method for testing the neutral mutation hypothesis by DNA polymorphism. *Genetics* **123**, 585–595 (1989). Medline

25. S. Guindon, J. F. Dufayard, V. Lefort, M. Anisimova, W. Hordijk, O. Gascuel, New algorithms and methods to estimate maximum-likelihood phylogenies: Assessing the performance of PhyML 3.0. *Syst. Biol.* **59**, 307–321 (2010). doi:10.1093/sysbio/syq010 Medline

26. B. Gallone, J. Steensels, T. Prahl, L. Soriaga, V. Saels, B. Herrera-Malaver, A. Merlevede, M. Roncoroni, K. Voordeckers, L. Miraglia, C. Teiling, B. Steffy, M. Taylor, A. Schwartz, T. Richardson, C. White, G. Baele, S. Maere, K. J. Verstrepen, Domestication and divergence of *Saccharomyces cerevisiae* beer yeasts. *Cell* **166**, 1397–1410.e16 (2016). doi:10.1016/j.cell.2016.08.020 Medline

27. M. C. Fisher, T. W. J. Garner, The relationship between the emergence of *Batrachochytrium dendrobatidis*, the international trade in amphibians and introduced amphibian species. *Fungal Biol. Rev.* **21**, 2–9 (2007). doi:10.1016/j.fbr.2007.02.002

28. A. I. Carpenter, F. Andreone, R. D. Moore, R. A. Griffiths, A review of the international trade in amphibians: The types, levels and dynamics of trade in CITES-listed species. *Oryx* **48**, 565–574 (2014). doi:10.1017/S0030605312001627

29. J. K. Pritchard, M. Stephens, P. Donnelly, Inference of population structure using multilocus genotype data. *Genetics* **155**, 945–959 (2000). Medline

30. S. J. Price, T. W. Garner, R. A. Nichols, F. Balloux, C. Ayres, A. Mora-Cabello de Alba, J. Bosch, Collapse of amphibian communities due to an introduced Ranavirus. *Curr. Biol.* **24**, 2586–2591 (2014). doi:10.1016/j.cub.2014.09.028 Medline

31. T. W. J. Garner, S. Walker, J. Bosch, S. Leech, J. M. Rowcliffe, A. A. Cunningham, M. C. Fisher, Life history tradeoffs influence mortality associated with the amphibian pathogen *Batrachochytrium dendrobatidis*. *Oikos* **118**, 783–791 (2009). doi:10.1111/j.1600-0706.2008.17202.x

32. K. A. Bates, F. C. Clare, S. O'Hanlon, J. Bosch, L. Brookes, K. Hopkins, E. J. McLaughlin, O. Daniel, T. W. J. Garner, M. C. Fisher, X. A. Harrison, Amphibian chytridiomycosis outbreak dynamics are linked with host skin bacterial community structure. *Nat. Commun.* **9**, 693 (2018). doi:10.1038/s41467-018-02967-w Medline

33. B. J. Doddington, J. Bosch, J. A. Oliver, N. C. Grassly, G. Garcia, B. R. Schmidt, T. W. Garner, M. C. Fisher, Context-dependent amphibian host population response to an invading pathogen. *Ecology* **94**, 1795–1804 (2013). doi:10.1890/12-1270.1 Medline

34. D. H. Olson, K. L. Ronnenberg, Global Bd Mapping Project: 2014 Update. *FrogLog* **22**, 17–21 (2014).

35. S. F. Walker, J. Bosch, T. Y. James, A. P. Litvintseva, J. A. Oliver Valls, S. Piña, G. García, G. A. Rosa, A. A. Cunningham, S. Hole, R. Griffiths, M. C. Fisher, Invasive pathogens threaten species recovery programs. *Curr. Biol.* **18**, R853–R854 (2008). doi:10.1016/j.cub.2008.07.033 Medline

36. E. L. Wombwell, T. W. J. Garner, A. A. Cunningham, R. Quest, S. Pritchard, J. M. Rowcliffe, R. A. Griffiths, Detection of *Batrachochytrium dendrobatidis* in amphibians imported into the UK for the pet trade. *EcoHealth* **13**, 456–466 (2016). doi:10.1007/s10393-016-1138-4 Medline

37. K. H. O'Rourke, J. G. Williamson, When did globalisation begin? *Eur. Rev. Econ. Hist.* **6**, 23–50 (2002). doi:10.1017/S1361491602000023

38. J. E. Kolby, Stop Madagascar's toad invasion now. *Nature* **509**, 563 (2014). doi:10.1038/509563a Medline

39. A. Herrel, A. van der Meijden, An analysis of the live reptile and amphibian trade in the USA compared to the global trade in endangered species. *Herpetol. J.* **24**, 103–110 (2014).

40. N. Dahanukar, K. Krutha, M. S. Paingankar, A. D. Padhye, N. Modak, S. Molur, Endemic Asian chytrid strain infection in threatened and endemic anurans of the Northern Western Ghats, India. *PLOS ONE* **8**, e77528 (2013). doi:10.1371/journal.pone.0077528 Medline

41. S. Molur, K. Krutha, M. S. Paingankar, N. Dahanukar, Asian strain of *Batrachochytrium dendrobatidis* is widespread in the Western Ghats, India. *Dis. Aquat. Organ.* **112**, 251–255 (2015). doi:10.3354/dao02804 Medline

42. C. Bai, X. Liu, M. C. Fisher, W. J. T. Garner, Y. Li, Global and endemic Asian lineages of the emerging pathogenic fungus *Batrachochytrium dendrobatidis* widely infect

amphibians in China. *Divers. Distrib.* **18**, 307–318 (2012). doi:10.1111/j.1472-4642.2011.00878.x

43. A. Martel, M. Blooi, C. Adriaensen, P. Van Rooij, W. Beukema, M. C. Fisher, R. A. Farrer, B. R. Schmidt, U. Tobler, K. Goka, K. R. Lips, C. Muletz, K. R. Zamudio, J. Bosch, S. Lötters, E. Wombwell, T. W. Garner, A. A. Cunningham, A. Spitzen-van der Sluijs, S. Salvidio, R. Ducatelle, K. Nishikawa, T. T. Nguyen, J. E. Kolby, I. Van Bocxlaer, F. Bossuyt, F. Pasmans, Recent introduction of a chytrid fungus endangers Western Palearctic salamanders. *Science* **346**, 630–631 (2014). doi:10.1126/science.1258268 Medline

44. H. E. Roy, H. Hesketh, B. V. Purse, J. Eilenberg, A. Santini, R. Scalera, G. D. Stentiford, T. Adriaens, K. Bacela-Spychalska, D. Bass, K. M. Beckmann, P. Bessell, J. Bojko, O. Booy, A. C. Cardoso, F. Essl, Q. Groom, C. Harrower, R. Kleespies, A. F. Martinou, M. M. van Oers, E. J. Peeler, J. Pergl, W. Rabitsch, A. Roques, F. Schaffner, S. Schindler, B. R. Schmidt, K. Schonrogge, J. Smith, W. Solarz, A. Stewart, A. Stroo, E. Tricarico, K. M. A. Turvey, A. Vannini, M. Vila, S. Woodward, A. A. Wynns, A. M. Dunn, Alien pathogens on the horizon: Opportunities for predicting their threat to wildlife. *Conserv. Lett.* **10**, 477–484 (2017). doi:10.1111/conl.12297

45. M. Martin, Cutadapt removes adapter sequences from high-throughput sequencing reads. *EMBnet J.* **17**, 10–12 (2011). doi:10.14806/ej.17.1.200

46. H. Li, Aligning sequence reads, clone sequences and assembly contigs with BWA-MEM. arXiv:1303.3997 (2013).

47. H. Li, B. Handsaker, A. Wysoker, T. Fennell, J. Ruan, N. Homer, G. Marth, G. Abecasis, R. Durbin, The sequence alignment/map format and SAMtools. *Bioinformatics* **25**, 2078–2079 (2009). doi:10.1093/bioinformatics/btp352 Medline

48. E. Garrison, G. Marth, Haplotype-based variant detection from short-read sequencing. arXiv:1207.3907 (2012).

49. E. Garrison, Vcflib: A C++ library for parsing and manipulating VCF files. GitHub https://github.com/ekg/vcflib (2012).

50. A. Tan, G. R. Abecasis, H. M. Kang, Unified representation of genetic variants. *Bioinformatics* **31**, 2202–2204 (2015). doi:10.1093/bioinformatics/btv112 Medline

51. A. Stamatakis, RAxML version 8: A tool for phylogenetic analysis and post-analysis of large phylogenies. *Bioinformatics* **30**, 1312–1313 (2014). doi:10.1093/bioinformatics/btu033 Medline

52. A. McKenna, M. Hanna, E. Banks, A. Sivachenko, K. Cibulskis, A. Kernytsky, K. Garimella, D. Altshuler, S. Gabriel, M. Daly, M. A. DePristo, The Genome Analysis Toolkit: A MapReduce framework for analyzing next-generation DNA sequencing data. *Genome Res.* **20**, 1297–1303 (2010). doi:10.1101/gr.107524.110 Medline

53. A. J. Drummond, M. A. Suchard, D. Xie, A. Rambaut, Bayesian phylogenetics with BEAUti and the BEAST 1.7. *Mol. Biol. Evol.* **29**, 1969–1973 (2012). doi:10.1093/molbev/mss075 Medline

54. D. Posada, K. A. Crandall, MODELTEST: Testing the model of DNA substitution. *Bioinformatics* **14**, 817–818 (1998). doi:10.1093/bioinformatics/14.9.817 Medline

55. A. Rieux, F. Balloux, Inferences from tip-calibrated phylogenies: A review and a practical guide. *Mol. Ecol.* **25**, 1911–1924 (2016). doi:10.1111/mec.13586 Medline

56. S. F. Walker, J. Bosch, V. Gomez, T. W. Garner, A. A. Cunningham, D. S. Schmeller, M. Ninyerola, D. A. Henk, C. Ginestet, C. P. Arthur, M. C. Fisher, Factors driving pathogenicity vs. prevalence of amphibian panzootic chytridiomycosis in Iberia. *Ecol. Lett.* **13**, 372–382 (2010). doi:10.1111/j.1461-0248.2009.01434.x Medline

57. N. Wales, C. Carøe, M. Sandoval-Velasco, C. Gamba, R. Barnett, J. A. Samaniego, J. R. Madrigal, L. Orlando, M. T. Gilbert, New insights on single-stranded versus double-stranded DNA library preparation for ancient DNA. *Biotechniques* **59**, 368–371 (2015). doi:10.2144/000114364 Medline

58. M. Schubert, L. Ermini, C. Der Sarkissian, H. Jónsson, A. Ginolhac, R. Schaefer, M. D. Martin, R. Fernández, M. Kircher, M. McCue, E. Willerslev, L. Orlando, Characterization of ancient and modern genomes by SNP detection and phylogenomic and metagenomic analysis using PALEOMIX. *Nat. Protoc.* **9**, 1056–1082 (2014). doi:10.1038/nprot.2014.063 Medline

59. S. Koren, B. P. Walenz, K. Berlin, J. R. Miller, N. H. Bergman, A. M. Phillippy, Canu: Scalable and accurate long-read assembly via adaptive *k*-mer weighting and repeat separation. *Genome Res.* **27**, 722–736 (2017). doi:10.1101/gr.215087.116 Medline

60. I. Sović, M. Šikić, A. Wilm, S. N. Fenlon, S. Chen, N. Nagarajan, Fast and sensitive mapping of nanopore sequencing reads with GraphMap. *Nat. Commun.* **7**, 11307 (2016). doi:10.1038/ncomms11307 Medline

61. B. J. Walker, T. Abeel, T. Shea, M. Priest, A. Abouelliel, S. Sakthikumar, C. A. Cuomo, Q. Zeng, J. Wortman, S. K. Young, A. M. Earl, Pilon: An integrated tool for comprehensive microbial variant detection and genome assembly improvement. *PLOS ONE* **9**, e112963 (2014). doi:10.1371/journal.pone.0112963 Medline

62. N. Beck, B. Lang, MFannot Tool; http://megasun.bch.umontreal.ca/cgi-bin/mfannot/mfannotInterface.pl.

63. P. Jones, D. Binns, H. Y. Chang, M. Fraser, W. Li, C. McAnulla, H. McWilliam, J. Maslen, A. Mitchell, G. Nuka, S. Pesseat, A. F. Quinn, A. Sangrador-Vegas, M. Scheremetjew, S. Y. Yong, R. Lopez, S. Hunter, InterProScan 5: Genome-scale protein function classification. *Bioinformatics* **30**, 1236–1240 (2014). doi:10.1093/bioinformatics/btu031 Medline

64. T. M. Lowe, P. P. Chan, tRNAscan-SE On-line: Integrating search and context for analysis of transfer RNA genes. *Nucleic Acids Res.* **44**, W54–W57 (2016). doi:10.1093/nar/gkw413 Medline

65. T. M. Lowe, S. R. Eddy, tRNAscan-SE: A program for improved detection of transfer RNA genes in genomic sequence. *Nucleic Acids Res.* **25**, 955–964 (1997). doi:10.1093/nar/25.5.0955 Medline

66. P. Danecek, A. Auton, G. Abecasis, C. A. Albers, E. Banks, M. A. DePristo, R. E. Handsaker, G. Lunter, G. T. Marth, S. T. Sherry, G. McVean, R. Durbin, The variant call format and VCFtools. *Bioinformatics* **27**, 2156–2158 (2011). doi:10.1093/bioinformatics/btr330 Medline

67. O. Delaneau, B. Howie, A. J. Cox, J. F. Zagury, J. Marchini, Haplotype estimation using sequencing reads. *Am. J. Hum. Genet.* **93**, 687–696 (2013). doi:10.1016/j.ajhg.2013.09.002 Medline

68. D. Falush, M. Stephens, J. K. Pritchard, Inference of population structure using multilocus genotype data: Linked loci and correlated allele frequencies. *Genetics* **164**, 1567–1587 (2003). Medline

69. G. Evanno, S. Regnaut, J. Goudet, Detecting the number of clusters of individuals using the software STRUCTURE: A simulation study. *Mol. Ecol.* **14**, 2611–2620 (2005). doi:10.1111/j.1365-294X.2005.02553.x Medline

70. X. Zheng, D. Levine, J. Shen, S. M. Gogarten, C. Laurie, B. S. Weir, A high-performance computing toolset for relatedness and principal component analysis of SNP data. *Bioinformatics* **28**, 3326–3328 (2012). doi:10.1093/bioinformatics/bts606 Medline

71. R Core Team (R Foundation for Statistical Computing, Vienna, 2017).

72. H. Wickham, *ggplot2: elegant graphics for data analysis*. *Use R!* (Springer, 2009).

73. K. L. Gosner, A simplified table for staging anuran embryos and larvae with notes on identification. *Herpetologica* **16**, 183–190 (1960).

74. D. G. Boyle, D. B. Boyle, V. Olsen, J. A. Morgan, A. D. Hyatt, Rapid quantitative detection of chytridiomycosis (*Batrachochytrium dendrobatidis*) in amphibian samples using real-time Taqman PCR assay. *Dis. Aquat. Organ.* **60**, 141–148 (2004). doi:10.3354/dao060141 Medline

75. K. M. Kriger, H. B. Hines, A. D. Hyatt, D. G. Boyle, J. M. Hero, Techniques for detecting chytridiomycosis in wild frogs: Comparing histology with real-time Taqman PCR. *Dis. Aquat. Organ.* **71**, 141–148 (2006). doi:10.3354/dao071141 Medline

76. P. Kleinhenz, M. D. Boone, G. Fellers, Effects of the amphibian chytrid fungus and four insecticides on Pacific treefrogs (*Pseudacris regilla*). *J. Herpetol.* **46**, 625–631 (2012). doi:10.1670/11-070

77. E. Luquet, T. W. Garner, J. P. Léna, C. Bruel, P. Joly, T. Lengagne, O. Grolet, S. Plénet, Genetic erosion in wild populations makes resistance to a pathogen more costly. *Evolution* **66**, 1942–1952 (2012). doi:10.1111/j.1558-5646.2011.01570.x Medline

78. M. J. Parris, T. O. Cornelius, Fungal pathogen causes competitive and developmental stress in larval amphibian communities. *Ecology* **85**, 3385–3395 (2004). doi:10.1890/04-0383

79. D. Darriba, G. L. Taboada, R. Doallo, D. Posada, ProtTest 3: Fast selection of best-fit models of protein evolution. *Bioinformatics* **27**, 1164–1165 (2011). doi:10.1093/bioinformatics/btr088 Medline

80. K. Tamura, G. Stecher, D. Peterson, A. Filipski, S. Kumar, MEGA6: Molecular Evolutionary Genetics Analysis version 6.0. *Mol. Biol. Evol.* **30**, 2725–2729 (2013). doi:10.1093/molbev/mst197 Medline

81. R. R. Wick, M. B. Schultz, J. Zobel, K. E. Holt, Bandage: Interactive visualization of de novo genome assemblies. *Bioinformatics* **31**, 3350–3352 (2015). doi:10.1093/bioinformatics/btv383 Medline

82. M. J. Laforest, I. Roewer, B. F. Lang, Mitochondrial tRNAs in the lower fungus *Spizellomyces punctatus*: tRNA editing and UAG ‘stop’ codons recognized as leucine. *Nucleic Acids Res.* **25**, 626–632 (1997). doi:10.1093/nar/25.3.626 Medline

83. E. Kayal, B. Bentlage, A. G. Collins, M. Kayal, S. Pirro, D. V. Lavrov, Evolution of linear mitochondrial genomes in medusozoan cnidarians. *Genome Biol. Evol.* **4**, 1–12 (2012). doi:10.1093/gbe/evr123 Medline

84. Z. Shao, S. Graf, O. Y. Chaga, D. V. Lavrov, Mitochondrial genome of the moon jelly *Aurelia aurita* (Cnidaria, Scyphozoa): A linear DNA molecule encoding a putative DNA-dependent DNA polymerase. *Gene* **381**, 92–101 (2006). doi:10.1016/j.gene.2006.06.021 Medline

85. M. Valach, Z. Farkas, D. Fricova, J. Kovac, B. Brejova, T. Vinar, I. Pfeiffer, J. Kucsera, L. Tomaska, B. F. Lang, J. Nosek, Evolution of linear chromosomes and multipartite genomes in yeast mitochondria. *Nucleic Acids Res.* **39**, 4202–4219 (2011). doi:10.1093/nar/gkq1345 Medline

86. C. A. Brewer, www.ColorBrewer.org (2018).

87. E. Neuwirth, RColorBrewer: ColorBrewer Palettes. R package version 1.1-2. https://CRAN.R-project.org/package=RColorBrewer (2014).

88. M. Dowle, A. Srinivasan, data.table: Extension of ‘data.frame’. R package version 1.10.4. https://CRAN.R-project.org/package=data.table (2017).

89. G. Yu, D. Smith, H. Zhu, Y. Guan, T. T.-Y. Lam, ggtree: An R package for visualization and annotation of phylogenetic trees with their covariates and other associated data. *Methods Ecol. Evol.* **8**, 28–36 (2017). doi:10.1111/2041-210X.12628

90. T. Galili, dendextend: An R package for visualizing, adjusting and comparing trees of hierarchical clustering. *Bioinformatics* **31**, 3718–3720 (2015). doi:10.1093/bioinformatics/btv428 Medline